Separation Science and Technology
Publication details, including instructions for authors and subscription information:
http://www.informaworld.com/smpp/title~content=t713708471

Hydraulic Permeability, Mass Transfer, and Retention of PEGs in Cross-flow Ultrafiltration through a Symmetric Microporous Membrane

P. Pradanos[a]; J. I. Arribas[a]; A. Hernandez[a]
[a] DEPARTAMENTO DE FÍSICA APLICADA II FACULTAD DE CIENCIAS, UNIVERSIDAD DE VALLADOLID, VALLADOID, SPAIN

To cite this Article Pradanos, P. , Arribas, J. I. and Hernandez, A.(1992) 'Hydraulic Permeability, Mass Transfer, and Retention of PEGs in Cross-flow Ultrafiltration through a Symmetric Microporous Membrane', Separation Science and Technology, 27: 15, 2121 — 2142
To link to this Article: DOI: 10.1080/01496399208019470
URL: http://dx.doi.org/10.1080/01496399208019470

SEPARATION SCIENCE AND TECHNOLOGY, **27**(15), pp. 2121–2142, 1992

Hydraulic Permeability, Mass Transfer, and Retention of PEGs in Cross-flow Ultrafiltration through a Symmetric Microporous Membrane

P. PRADANOS, J. I. ARRIBAS, and A. HERNANDEZ*

DEPARTAMENTO DE FÍSICA APLICADA II
FACULTAD DE CIENCIAS
UNIVERSIDAD DE VALLADOLID
47071 VALLADOLID, SPAIN

Abstract

The flow and retention of 0.1% w/w aqueous solutions of several polyethylene glycols with molecular weights ranging from 3,000 to 35,000 dalton are studied when they are tangentially filtered through a nuclear track-etched symmetric microporous membrane made from polycarbonate with transmembrane pressure differences going up to 200 kPa. The work was done within the framework of the film layer theory for the concentration polarization phenomenon which allows one to obtain the mass transfer coefficient for the cell used as a function of the feed circulation speed and the molecular weight of the solute. The retention curves obtained lead to a sieve radius smaller than the nominal one.

INTRODUCTION

Ultrafiltration is being used increasingly as a concentration and separation process in a variety of industries. Ultrafiltration is amenable to both continuous and batch operations and offers several advantages over more traditional separation methods. For example, because there is no heat added, ultrafiltration is suitable for heat labile substances. In addition, products are not subjected to chemical denaturation which can occur with solvent extraction. However, application of ultrafiltration is limited by the permeability versus molecular weight characteristics of commercially available devices.

Manufacturers of ultrafilters generally specify a nominal "cut-off" for their products for use in process design. However, in practice this is not

*To whom correspondence should be addressed.

a sharply defined molecular weight below which solutes pass the membrane and above which they are retained. Rather, there is a gradual shift from free permeability to retention as molecular weight increases.

The permeation versus molecular weight behavior actually depends on the process parameters and device characteristics. Therefore, it depends on the concrete characteristics of the process and cell where the membrane is used.

Polyethylene glycols are good probe solutes, given that they are water soluble and can be readily obtained with narrow molecular weight distributions, which makes them a good selection to characterize a membrane-cell ensemble.

A tangentially driven device seems to have some advantages over dead-end designs, mainly due to its ability to limit the formation of a concentration polarization layer and consequently the fouling limits to permeation. In this case the molecular weight cutoff has to be carefully defined and studied in terms of the pressure difference allowed to act through the membrane and the velocity of recirculation used in the retentate loop. The influence of these parameters for a tangentially driven device with a symmetric track etched membrane of polycarbonate is studied here.

EXPERIMENTAL

Materials and Experimental Setup

A Nuclepore filter was used. It will be called N015 on account of its nominal pore diameter of 0.015 μm. It belongs to a gamut of microporous filters characterized by their regular structure with a very narrow distribution of pore sizes. They are obtained by a track etching process from very thin (6.36 ± 0.05 μm for the N015) polycarbonate sheets. In order to avoid any irreversible change during operation, each membrane sample has been pressurized at 200 kPa for 2 h before being used (higher pressures would damage the membrane, while no permeability change could be detected for longer pressurizing periods).

Aqueous solutions of several polyethylene glycols (PEGs) at 0.100% w/w were used. Their relatively small concentration assures minimal solute–solute interactions. They were prepared with distilled, degasified, and deionized (resistivity higher than 18 MΩ·cm) water, and seven different PEGs with molecular weights (MW) of 2,000, 3,000, 4,000, 6,000, 10,000, 12,000, and 35,000 dalton were supplied by Fluka AG.

The solutions are tangentially driven over the membrane and recirculated with several speeds, v, while the transmembrane pressure, Δp, goes up to 200 kPa.

The tangential ultrafiltration device used is shown in Fig. 1. The solution is extracted from a thermostated reservoir at 298 K by means of a regulatable impulsion pump. Two pressure transducers are placed before and after the membrane holder in the retentate loop; they have a range of 0–1000 kPa relative to the atmosphere and give a maximum error of ±0.25% full scale. Given that the permeate loop is open and the pressure loss along the hydraulic channel is small and almost linear, the transmembrane pressure can be taken as the average of the values given up and down the membrane cell. In order to measure the retentate flow, two electromagnetic flowmeters are alternatively used, whose ranges are from 1×10^{-6} to 1×10^{-5} m^3/s and from 8×10^{-5} to 1.67×10^{-4} m^3/s, both with errors lower than ±0.25% full scale. The speed and pressure in the retentate loop are independently controlled by means of pump regulation and a needle valve.

The permeate flux is measured by timing and weighing with a high precision balance with errors lower than $\pm 1 \times 10^{-7}$ kg. The concentration

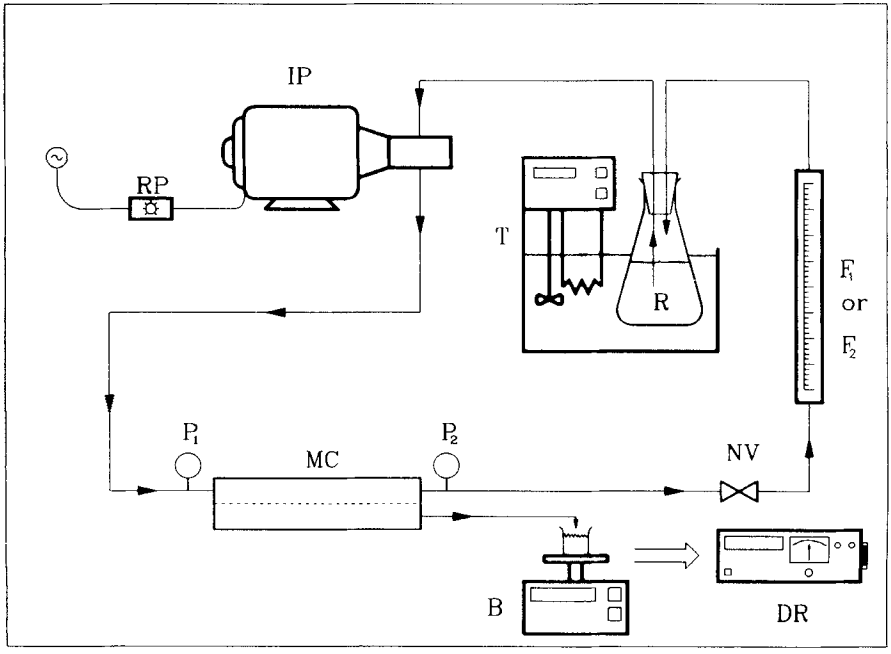

FIG. 1. Experimental device with thermostat (T), feed reservoir (R), pump regulator (RP), impulsion pump (IP), pressure transducers (P_1, P_2), membrane cell (MC), needle value (NV), flowmeters (F_1 or F_2), balance (B), and differential refractometer (DR).

of the permeate is measured by using a previously calibrated differential refractometer with the same high quality water used to prepare the filtered solutions as reference. The calibration ranges went from 0.04 to 1% w/w, and only the linear refractive index versus concentration domains are used by controlled dilution or concentration of each sample.

The membrane cell is schematically shown in Fig. 2. On the membrane, there are four prismatic channels of length $L = 28.0 \times 10^{-3}$ m and the transversal dimensions 1.00×10^{-3} m and 5.25×10^{-3} m, whose hydraulic diameter is $d_h = 1.68 \times 10^{-3}$ m, giving an effective membrane area of 5.08×10^{-4} m^2 and a total retentate loop cross section of 9.00×10^{-6} m^2.

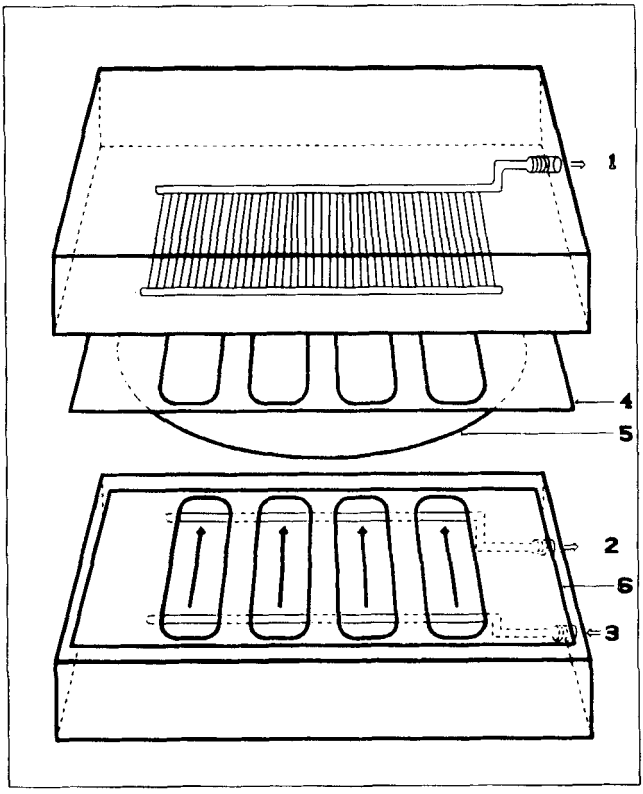

FIG. 2. Membrane holder showing the permeate output (1), the retentate output (2), the feed input (3), the permeate separator (4), the membrane (5), and the retentate separator (6).

Volume Flow and Hydraulic Permeability

First of all, the volume flow of permeate, J_v, has been measured as a function of transmembrane pressure for pure water and the seven PEGs solutions used, while the average retentate recirculation speed was kept constant at the following values: 0.024, 0.040, 0.080, 0.120, 0.160, 0.400, 0.790, and 2.143 m/s. The pure water volume flow is independent of the tangential speed and is shown against the transmembrane pressure in Fig. 3. In any case, there is a low pressure zone where the plot is not linear, leading to a dependence of the Swartzendruber type (*1*), i.e.,

$$J_v = L_p\Delta p - L_p p_0(1 - e^{-\Delta p/p_0}) \tag{1}$$

For $\Delta p \gg p_0$, this leads to

$$J_v = L_p(\Delta p - p_0) \tag{2}$$

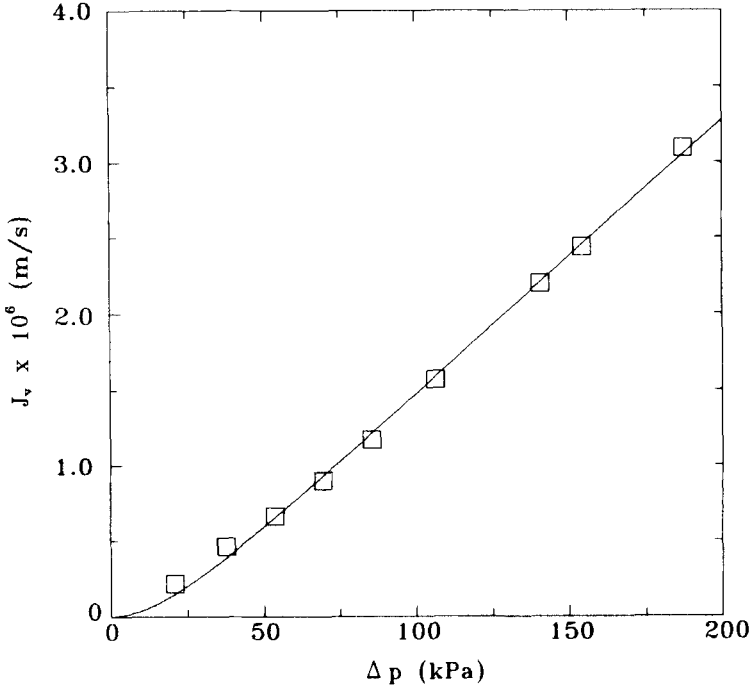

FIG. 3. Pure water volume flow versus the transmembrane pressure. The experimental points are fitted using Eq. (1) with p_0 = 18,000 kPa and L_p = 1.8076 × 10^{-11} m/Pa·s.

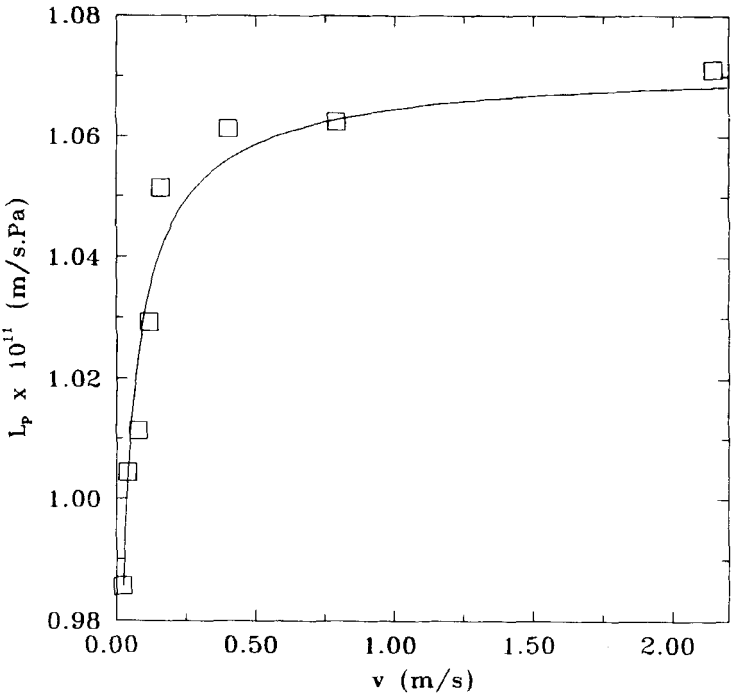

FIG. 4. The hydraulic permeability as a function of speed for PEG-35000. The curve drawn here corresponds to $L_p = 1.0711 \times 10^{-11}[1 - \exp(-av^b)]$ with $a = 5.08 \pm 0.39$ and $b = 0.191 \pm 0.025$.

The hydraulic permeability, L_p, increases with velocity for any solute, while for a fixed speed it decreases with the molecular weight of the solute. As an example, L_p is shown as a function of speed for PEG-35000 in Fig. 4, while it is plotted versus the molecular weight for $v = 2.143$ m/s in Fig. 5. On the other hand, the threshold pressure p_0 is constant, within the error range, for any solute and speed with an averaged value of $p_0 = 11.6 \pm 0.5$ kPa.

Observed Retention

Concerning the output or permeate concentration, c_p, it is convenient to give it in terms of the input or retentate concentration, c_0, through the so-called observed or apparent retention coefficient

$$R_o = 1 - \frac{c_p}{c_0} \tag{3}$$

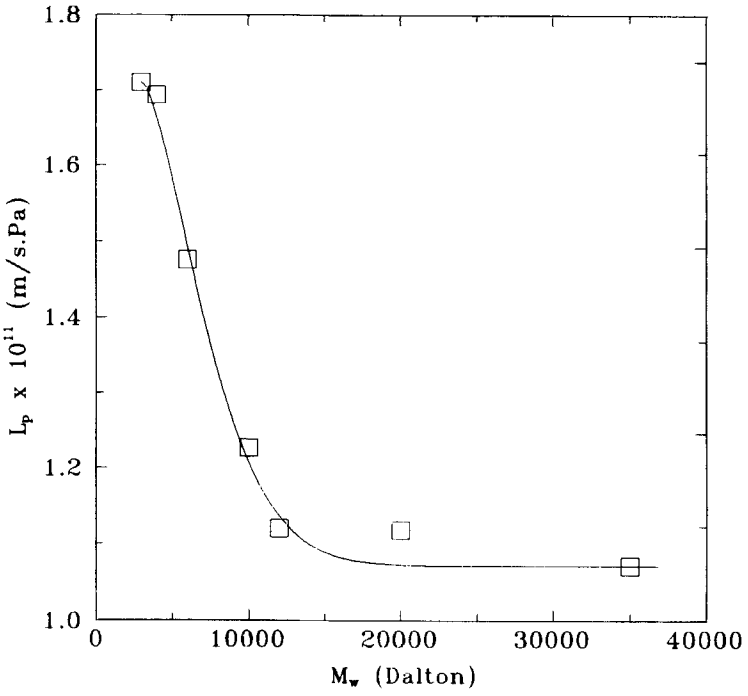

FIG. 5. The hydraulic permeability as a function of the molecular weight for a speed v = 2.143 m/s. The fitted curve is $L_p = a_1 + a_2 \exp(-a_3 M_w^b)$ with $a_1 = (1.093 \pm 0.024) \times 10^{-11}$, $a_2 = (0.711 \pm 0.085) \times 10^{-11}$, $a_3 = (1.05 \pm 0.01) \times 10^{-9}$, and $b = 2.31 \pm 0.56$.

This retention coefficient is, in principle, a function of pressure, recirculation speed, and molecular weight (*2–4*). Clearly, it decreases with Δp while it increases with M_w and v. In Fig. 6 the apparent retention is plotted versus pressure for the eight speeds used and PEG-35000. it is seen that there is invariably a linear zone for low Δp which is wider for the higher velocity. A tendency to limit R_o is observed so that $v > 2.143$ m/s doesn't give significantly higher retention coefficients, as will be seen below. For this maximal recirculation speed, R_o is shown in Fig. 7 as a function of Δp for the seven studied PEGs.

THEORY

Concentration Polarization

Due to the so-called concentration polarization, it has to be assumed that in contact with the membrane there is a concentration $c_m > c_0$ due to

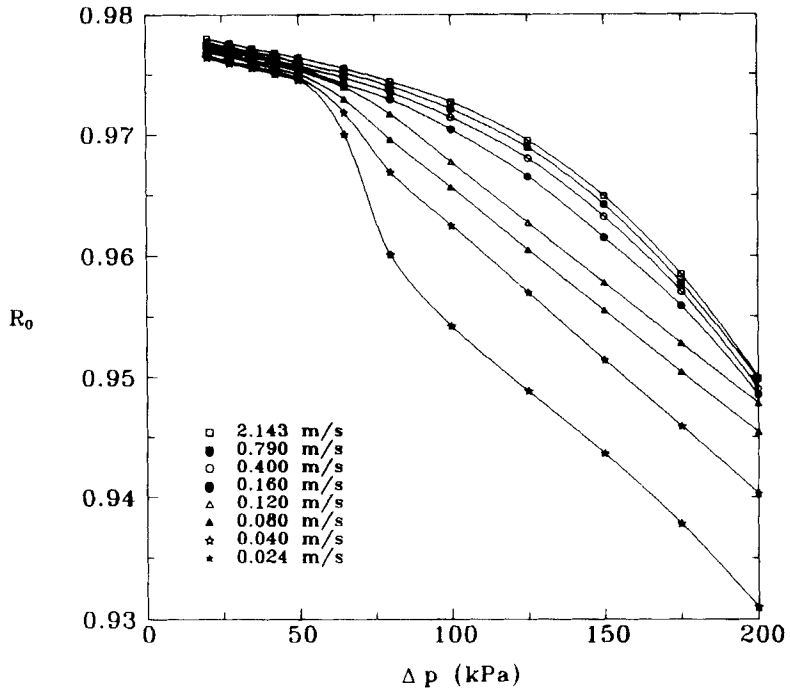

FIG. 6. The observed retention coefficient as a function of pressure for the eight recirculation speeds used and PEG-35000.

an accumulation phenomenon resulting from the balance of convection through the membrane and backdiffusion. This can be studied by following the so-called film-layer model (*5*) which assumes that there is a zone where the concentration decreases from c_m at the membrane to c_0 at a distance δ inside the retentate phase. This hypothesis leads to (*6–9*)

$$J_v = K_m \ln \frac{c_m - c_p}{c_0 - c_p} \tag{4}$$

where $K_m = D/\delta$ is called the mass transfer coefficient and D is the diffusion coefficient.

If a true retention coefficient is defined as

$$R = 1 - \frac{c_p}{c_m} \tag{5}$$

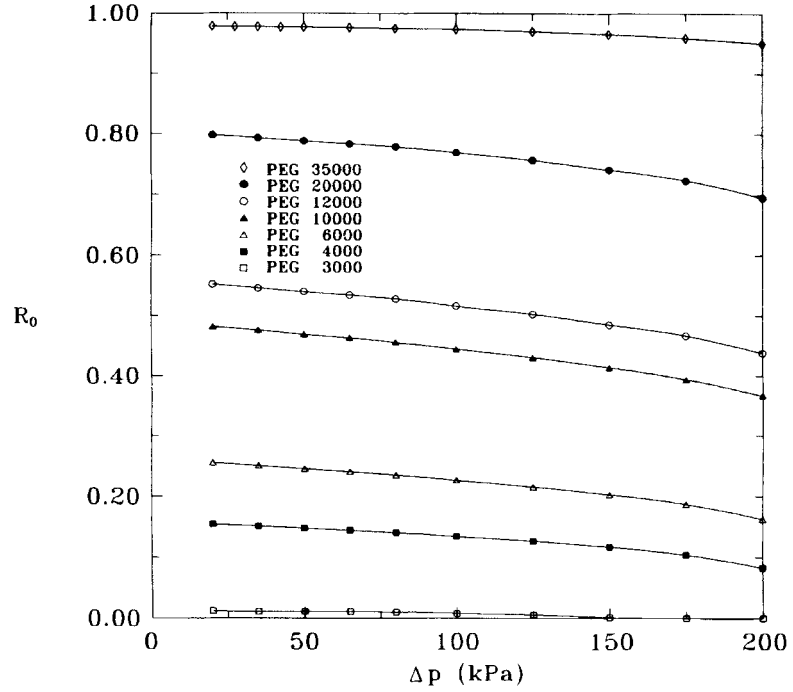

FIG. 7. The observed retention coefficient as a function of pressure for the seven PEGs studied and $v = 2.143$ m/s.

Eq. (4) can be modified to

$$\ln \frac{1 - R_o}{R_o} = \ln \frac{1 - R}{R} + \frac{J_v}{K_m} \tag{6}$$

Then, if c_m goes to a maximum, which should correspond to the formation of a gel layer, c_p/c_m is almost constant. Therefore, the first term of the right-hand side of Eq. (6) changes very slowly. Thus, a plot of ln $[(1 - R_o)/R_o]$ against J_v would be straight for high volume flows. Its slope would be $1/K_m$ and its ordinate intercept would give the maximum true retention coefficient. Nevertheless, this gelification should give a plateau for J_v versus Δp for high pressures, which is not seen for the PEGs and pressures used.

If the plot is tried in our conditions, what we get are the curves of Figs. 8 and 9. In any case, there is a linear zone for low volume flows or, what is the same thing, small transmembrane pressure drops. For these low J_v, what probably happens is that c_p increases linearly with c_m; thus, ln [(1 −

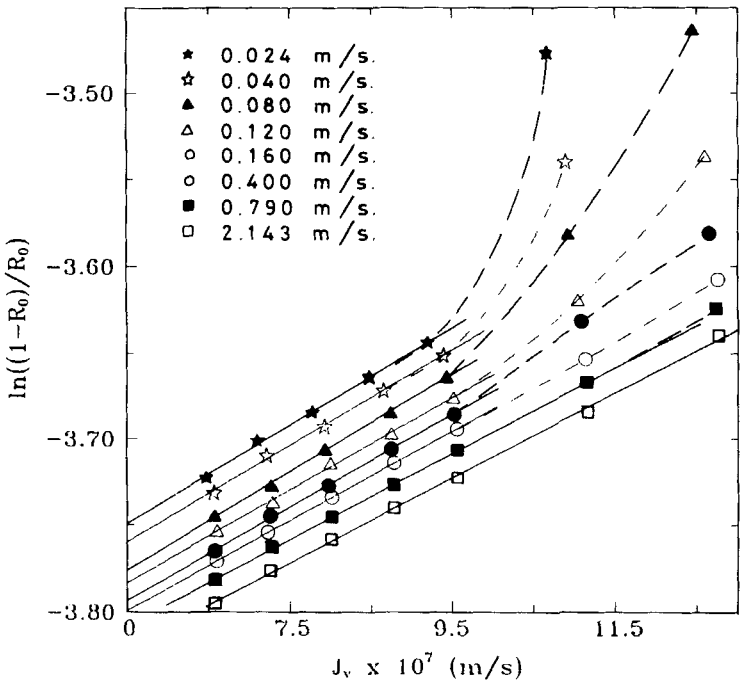

FIG. 8. Ln $[(1 - R_o)/R_o]$ as a function of J_v for PEG-35000 and the eight recirculation speeds used. Only the linear zones are shown here.

$R)/R]$ is also constant and Eq. (6) can be used to identify the slope of the low J_v linear zone with $1/K_m$, while the ordinate intercept is not related to the maximum but with the initial true retention coefficient.

Mass Transfer Coefficient and Analogies

According to the method outlined, the mass transfer coefficient can be easily calculated. The dependence of K_m on the recirculation speed is usually given by some kind of combination of dimensionless numbers (*2*, *10*) as

$$\mathrm{Sh} = A(\mathrm{Re})^{\alpha}(\mathrm{Sc})^{\beta} \tag{7}$$

where A, α, and β are constants, and the Sherwood, Reynolds, and Schmidt numbers are

$$\mathrm{Sh} = K_m d_h / D$$

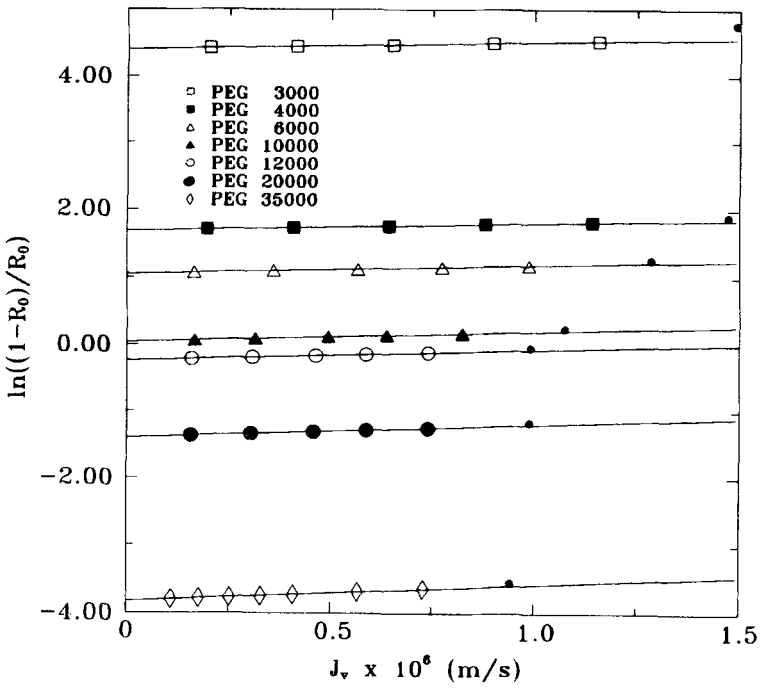

FIG. 9. Ln $[(1 - R_o)/R_o]$ as a function of J_v for the seven PEGs studied and v = 2.143 m/s. Just the linear zones are drawn here. The small, filled circles correspond to the first experimental points out of the linear domains.

$$\mathrm{Re} = v\rho d_h/\eta$$

$$\mathrm{Sc} = \eta/\rho D$$

with ρ being the density of the retentate solution and η its viscosity, whose values are taken as equal to the pure-water ones at 298.0 K, i.e., ρ = 997.07 kg/m^3 and $\eta = 0.8937 \times 10^{-3}$ kg/m·s. The values of the diffusion coefficient of PEGs at the same temperature, as taken from the literature (*11*), are shown in Table 1.

In Fig. 10, K_m is shown as a function of v for M_w = 35,000; while in Fig. 11 it is plotted versus M_w for v = 2.143 m/s. The curves in both figures correspond to

$$\mathrm{Sh} = 3.53(\mathrm{Re})^{0.04}(\mathrm{Sc})^{0.36} \tag{8}$$

with $A = 3.53 \pm 0.06$, $\alpha = 0.039 \pm 0.002$, and $\beta = 0.357 \pm 0.001$ that have been obtained by a nonlinear fitting procedure of the Marquardt type.

TABLE 1
The Diffusion Coefficients of PEGs as Taken from the Literature. They Can Be Fitted to $D = aM_w^b$ with $a = (9.82 \pm 0.96) \times 10^{-9}$ and $b = -(0.52 \pm 0.01)$

M_w (dalton)	D (10^{-11} m^2/s)
3,000	14.86
4,000	12.82
6,000	9.98
10,000	7.90
12,000	7.35
20,000	5.56
35,000	4.01

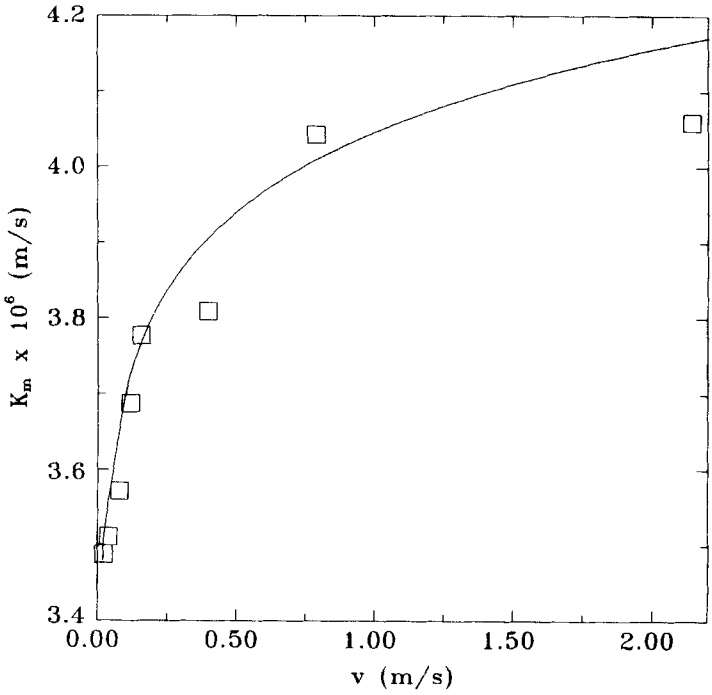

FIG. 10. The mass transfer coefficient as a function of v for $M_w = 35{,}000$.

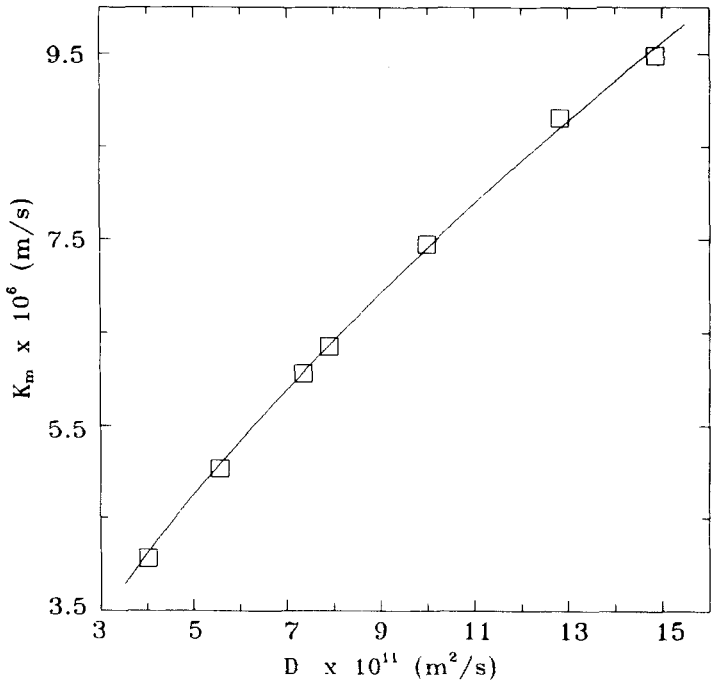

FIG. 11. The mass transfer coefficient as a function of D for v = 2.143 m/s.

True Retention and Membrane Concentration

The true retention coefficient can be calculated for each mass transfer coefficient, according to Eq. (6), as a function of pressure (or alternatively J_v). The results so obtained are shown for M_w = 35,000 and the eight recirculation speeds studied in Fig. 12, and with v = 2.143 m/s for the seven PEGs in Fig. 13. In these figures it is seen that the initial true retention coefficient results are the maximal ones for the pressure range used. The membrane concentration c_m can be calculated from R, and it is shown in Figs. 14 and 15 as a function of volume flow.

In Fig. 12 it is seen that the maximal true retention is obtained for v = 2.143 m/s. Therefore, for this recirculation speed, the corresponding standard retention curves can be obtained if R is plotted against log M_w for each transmembrane pressure. They are shown in Fig. 16 for Δp = 20 and 200 kPa.

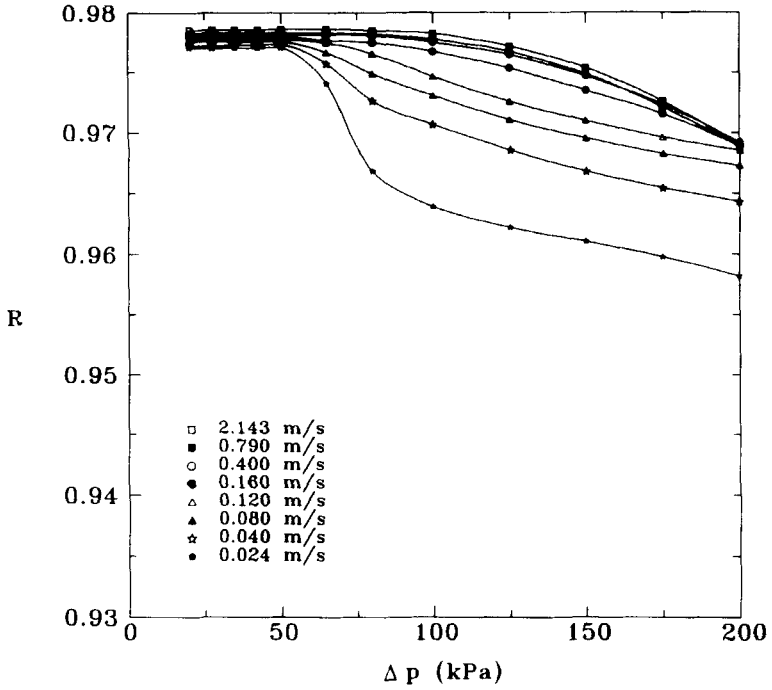

FIG. 12. True retention coefficient, R, as a function of transmembrane pressure for PEG-35000 and the eight speeds.

DISCUSSION AND CONCLUSIONS

Flow versus Pressure

Concerning the volume flow dependence on pressure, the Swartzendruber phenomenological equation can be attributed to a hydrophobic membrane matrix (*12*). Nevertheless, the wetting–drying process is usually associated with a more or less significant hysteresis which is not observed with N015 as was foreseeable because its polycarbonate matrix seems to be hydrophilic rather than hydrophobic.

In spite of the fact that this nonlinear dependence of the transmembrane average speed on the pressure drop across the membrane is also typical of non-Newtonian flow through a nondeformable porous body (*1*, *10*), this can be discarded given that substantially the same phenomenon is present with pure water as for PEG aqueous solutions, and that their concentrations are too low to present high non-Newtonian viscosity.

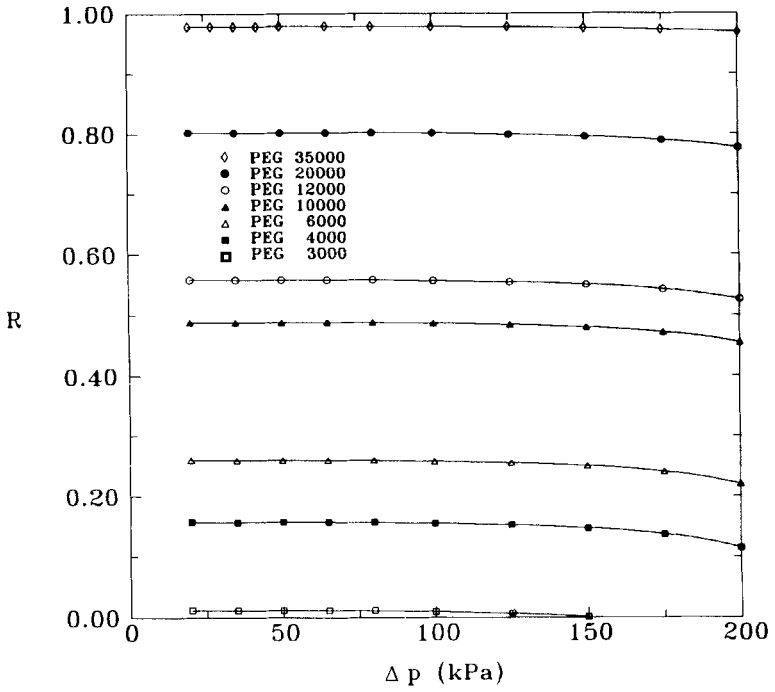

FIG. 13. True retention coefficient, R, as a function of transmembrane pressure for $v = 2.143$ m/s and the seven PEGS.

On the other hand, the almost equal value of p_0 for all the experiments should betoken an underlying structure-dependent process (*13*) like an elastic reversible deformation or even irreversible pore growth. These kinds of elasticity-connected phenomena are reversible until a threshold pressure is reached, which in our case ought be far above 200 kPa. The process seems to depend in a complex way on the initial pore radius, the pore density, and the working surface of the sample (*14*).

According to the Hagen–Poiseuille equation,

$$J_v = \frac{\epsilon r^2}{8\eta \Delta x} \Delta p \tag{9}$$

where ϵ is the porosity of fraction of void volume of the membrane, Δx is the membrane thickness, and η is the solution viscosity. Given that ϵ and Δx are known to be 0.0042 and 6.36×10^{-6} m respectively, Eq. (9) can be applied to the water volume flow (Fig. 3) to obtain $r(\Delta p = 0) =$

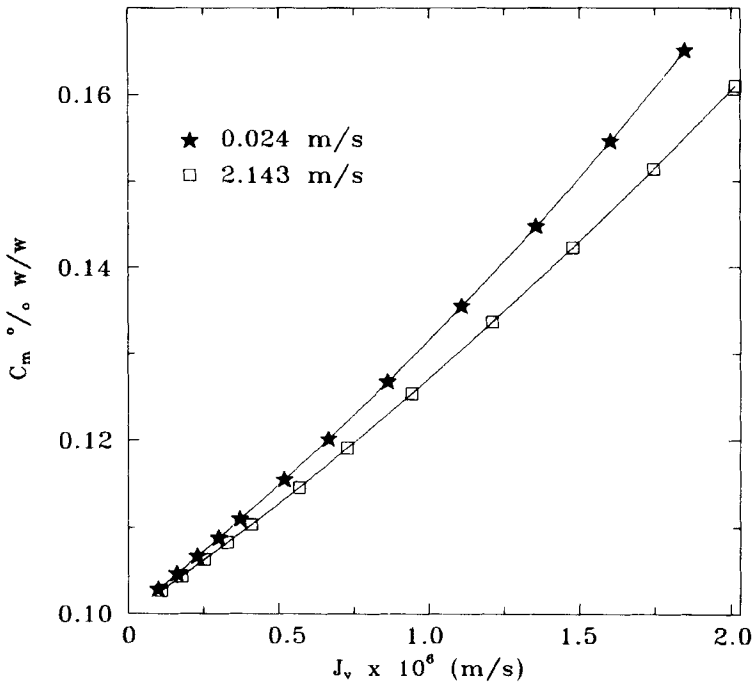

FIG. 14. Concentration on the retentate face of the membrane, c_m, as a function of J_v for PEG-35000 and the lower (0.024 m/s) and higher speeds (2.143 m/s).

1.147×10^{-8} m. Then we can assume that the membrane thickness as well as the number of pores per surface unit

$$N = \epsilon/\pi r^2 \tag{10}$$

are constant when Δp increases. But $N = 1.016 \times 10^{13}$ pores/m^2 according to Eq. (10). Thus, again using Eq. (9) but for high Δp we get $r(\Delta p = 200$ kPa$) = 1.267 \times 10^{-8}$ m and $\epsilon(\Delta p = 200$ kPa$) = 0.0051$; i.e., an increase of 25% in the pore radius along with a growth of 21% in porosity.

Hydraulic Permeability

The limiting hydraulic permeability that we have called L_p increases with the average speed in the retentate loop while it decreases with the PEG molecular weight, which seems reasonable (*15–19*). The fitted analytical dependencies shown in Figs. 4 and 5 are purely phenomenological, but they show that L_p goes to the pure water value for M_w going to zero, as

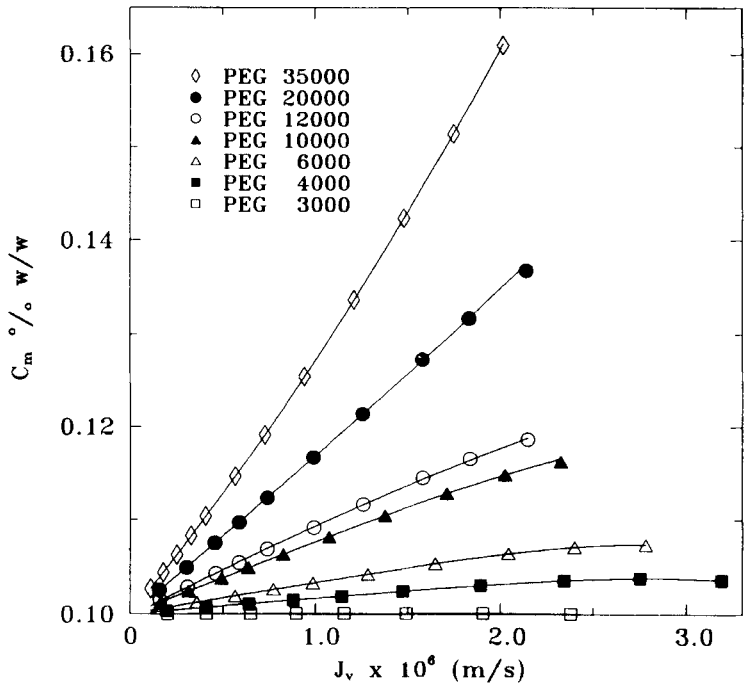

FIG. 15. Concentration of the retentate face of the membrane, c_m, as a function of J_v for $v = 2.143$ m/s and the seven PEGS.

was foreseeable. Of course, for v going to infinity, a limiting value should be reached which depends on M_w in such a way that this limit would increase until the pure water permeability for M_w goes to zero, giving a lower dependence on v until for pure water this dependence is almost nonexistent.

Some authors (*20*, *21*) have proposed other dependencies for the time-independent portion of the hydraulic permeability, namely

$$L_p = \frac{1}{R_m + R_{cp}} = \frac{1}{R_m + av^{b_1}(\Delta p)^{b_2}c_p^{b_3}} \tag{11}$$

for each M_w and c_0, where R_{cp} is the concentration-polarization resistance while R_m is the membrane resistance, which is the inverse of the pure water hydrodynamic permeability. Nevertheless, by definition L_p is pressure independent, hence Eq. (11) implies a power dependence of c_p on Δp, which is not the case for any PEG and recirculation speeds, as can be seen in Figs. 6 and 7 if Eq. (3) is taken into account.

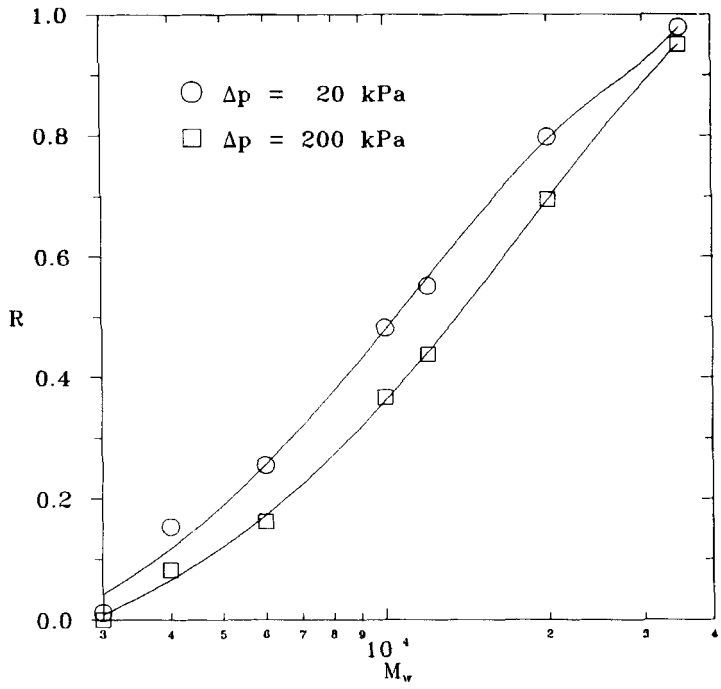

FIG. 16. Retention curves for Δp = 20 and 200 kPa and v = 2.143 m/s.

Mass Transfer Coefficients

Several values have been proposed for the coefficients A, α, and β. They can be calculated depending on the flow regime and the relation between the lengths of development of the limit layers for concentration L_c and momentum L_v and the channel length L for a laminar flow (*2*), leading to the results shown in Table 2. It is seen that A increases and α decreases

TABLE 2
The Coefficients of the Mass Transfer Correlation for Laminar and Turbulent Regimes

Flow regime	A	α	β		
Laminar	—	0	0	$L_v < L, L_c < L$	
	1.86	1/3	1/3	$L_v < L, L_c > L$	Graetz-Leveque
	0.664	1/2	1/3	$L_v > L, L_c > L$	Grober
Turbulent	0.023	0.8	1/3		Dittus-Boelter

when v decreases, while β remains constant except for very small values of v. We obtained $A = 3.53 \pm 0.06$, $\alpha = 0.039 \pm 0.002$, and $\beta = 0.357 \pm 0.001$, which are reasonable on account of the speed ranges analyzed.

In order to approach the turbulent state in the flow channel and therefore go to Dittus–Boelter conditions, some higher recirculation speeds were tested. In Fig. 17 the mass transfer coefficient is shown versus the recirculation speeds for $v = 2.143$, 3.175, 3.968, and 4.762 m/s along with the zone covered by the extreme bounds of the Dittus–Boelter correlation (*2*, *22*). It is seen how the Dittus–Boelter zone is reached for these very high speeds.

In fact, in spite of the higher mass transfer coefficients found for those higher recirculation speeds, they don't imply significantly higher R_o or R, as mentioned before. In effect, R_o increases with v for a fixed Δp but in such a way that a plateau is observed; for example, for $\Delta p = 65$ kPa the slope $\partial R_o/\partial v$ is 0.127 for $v = 0.24$ m/s, 3.352×10^{-4} for $v = 2.143$ m/s, and only 1.168×10^{-4} for $v = 4.762$ m/s.

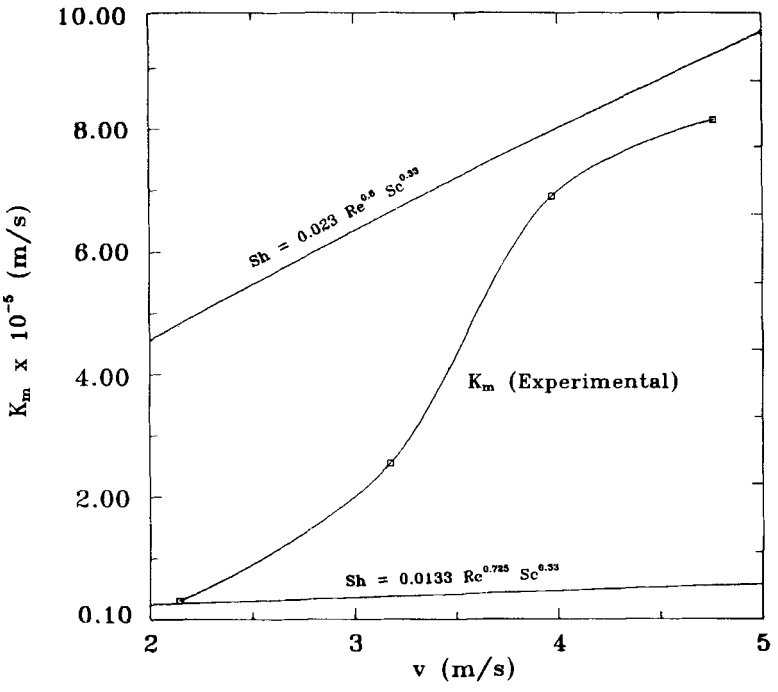

FIG. 17. K_m as a function of v for PEG-35000, showing how the Dittus–Boelter correlation is reached for very high speeds.

Retention Curves

As far as the retention curves are concerned, it seems that PEG-35000 is totally retained, which implies a pore radius given by (*23*)

$$r_s = (0.262\sqrt{M_w} - 0.3)1 \times 10^{-10} \tag{12}$$

where r_s is the gyration radius of the solute while M_w is in daltons, leading to $r_s = 0.487 \times 10^{-8}$. This is nearly 0.4 times the mean hydrodynamic radius and 0.7 times the nominal one. These differences could probably be explained by taking into account pore–solute friction and other solute–wall interaction factors. In fact, it is known that the hydrodynamic radius is systematically greater than the sieve-determined one, which is closer to the surface openings size. The difference is probably due to the existence of inner widenings of the pores. On the other hand, the nominal one is usually measured by experiments on the dead-end microfiltration of latex spheres. Hence, the smaller pore radius obtained can be a consequence of the special features of tangential microfiltration as well as of specific PEG–surface and PEG–PEG interactions which should be higher than for latex on account of their linear structure.

SYMBOLS

a, a_1, a_2, a_3	fitted constants
A	factor of the mass transfer correlation (dimensionless)
b, b_1, b_2, b_3	fitted constants
c_m	membrane concentration in contact with the high pressure interface (mol/m^3)
c_0	feed concentration (mol/m^3)
c_p	permeate concentration (mol/m^3)
d_h	diameter of the hydraulic channel (m)
D	diffusion coefficient (m^2/s)
J_v	volume flow per unit of area and time through the membrane (m/s)
K_m	mass transfer coefficient (m/s)
L	length of the hydraulic channel (m)
L_c	length of development of the concentration limit layer along the channel (m)
L_p	hydraulic permeability (m/Pa·s)
L_v	length of development of the velocity limit along the channel (m)
M_w	molecular weight (Dalton)
N	number of pores per surface unit (m^{-2})
p_0	parameter of the Swartzendruber equation (Pa)

r	pore radius (m)
r_s	gyration radius of the solute (m)
R	true retention coefficient (dimensionless)
R_o	observed retention coefficient (dimensionless)
R_{cp}	concentration polarization resistance (Pa·s/m)
R_m	membrane resistance (Pa·s/m)
Re	Reynolds number (dimensionless)
Sc	Schmidt number (dimensionless)
Sh	Sherwood number (dimensionless)
v	recirculation speed in the retentate loop (m/s)
α	exponent of the Reynolds number in the mass transfer correlation (dimensionless)
β	exponent of the Schmidt number in the mass transfer correlation (dimensionless)
δ	thickness of the concentration polarization film layer (m)
Δp	pressure drop through the membrane (Pa)
Δx	membrane thickness (m)
ϵ	porosity (dimensionless)
ρ	solution density (kg/m^3)
η	solution viscosity (kg/m·s)

REFERENCES

1. B. V. Derjaguin and N. V. Churaev, "Structure of the Boundary Layers of Liquids and Its Influence on the Mass Transfer in Fine Pores," *Prog. Surf. Membr. Sci., 14* (1981).
2. M. Cheryan, *Ultrafiltration Handbook,* Technomic, Lancaster, United Kingdom, 1986.
3. S. Nakao and S. Kimura, "Analysis of Solutes Rejection in Ultrafiltration," *J. Chem. Eng. Jpn., 14*(1), 32 (1981).
4. S. Nakao, J. G. Wijmans, and C. A. Smolders, "Resistance to the Permeate Flux in Unstirred Ultrafiltration of Dissolved Macromolecular Solutions," *J. Membr. Sci., 26,* 165 (1986).
5. C. K. Colton, S. Friedman, D. E. Wilson, and R. S. Lees, "Ultrafiltration of Lipoproteins through a Synthetic Membrane," *J. Clin. Invest., 51,* 2472 (1972).
6. S. Kimura and S. Nakao, "Fouling of Cellulose Acetate Tubular Reverse Osmosis Modules Treating the Industrial Water in Tokyo," *Desalination, 17,* 267 (1975).
7. G. Jonsson, "Transport Phenomena in Ultrafiltration: Membrane Selectivity and Boundary Layer Phenomena," *Pure Appl. Chem., 58,* 1647 (1986).
8. G. Jonsson and C. E. Boesen, "Concentration Polarization in a Reverse Osmosis Test Cell," *Desalination, 21,* 1 (1977).
9. G. Jonsson and P. M. Christensen, "Separation Characteristics of Ultrafiltration Membranes," in *Membranes and Membrane Processes* (E. Drioli and M. Nakagaki, eds.), Plenum Press, New York, 1984.
10. R. B. Bird, W. E. Stewart, and E. N. Lightfoot, *Transport Phenomena,* Wiley, New York, 1960.
11. J. Brandrup and E. H. Immergut (eds.), *Polymer Handbook,* Wiley, New York, 1989.

12. M. Mulder, *Basic Principles of Membrane Technology,* Kluwer, Dordrecht, The Netherlands, 1991.
13. V. I. Kuznetsov, V. V. Ovchinnikov, B. T. Porodnov, et al., "Investigation of Deformation Processes in a Loaded Nuclear Track Membrane," *J. Appl. Mech. Tech. Phys. (Engl. Transl.), 3,* 144 (1989).
14. V. V. Ovchinnikov, V. D. Seleznev, V. V. Surguchev, and V. I. Kuznetsov, "Controllable Changes in the Porous Structure of Polymeric Nuclear Track Membranes," *J. Membr. Sci., 55,* 299 (1991).
15. A. Bottino, G. Capannelli, A. Imperato, and S. Munari, "Ultrafiltration of Hydrosoluble Polymers. Effect of Operating Conditions on the Performance of the Membrane," *Ibid., 21,* 247 (1984).
16. R. Rautenbach and G. Schock, "Ultrafiltration of Macromolecular Solutions and Crossflow Microfiltration of Colloidal Suspensions. A Contribution to Permeate Flux Calculations," *Ibid., 36,* 231 (1988).
17. R. Nobrega, H. de Balmann, P. Aimar, and V. Sanchez, "Transfer of Dextran through Ultrafiltration Membranes. A Study of Rejection Data Analysed by Gel Permeation Chromatography," *Ibid., 45,* 17 (1989).
18. Q. T. Nguyen, P. Aptel, and J. Neel, "Characterization of Ultrafiltration Membranes. Part II. Mass Transport Measurements for Low and High Molecular Weight Synthetic Polymers in Water Solutions," *Ibid., 7,* 141 (1980).
19. S. Poyen, B. Bariou, N. Mameri, M. Portier, and M. Bergez, "Predictions of Rejection Coefficients in Ultrafiltration," *Ibid., 43,* 47 (1989).
20. J. Hiddink, R. de Boer, and P. F. C. Nooy, "Reverse Osmosis of Dairy Liquids," *J. Dairy Sci., 63,* 204 (1980).
21. A. J. B. Van Boxtel, Z. E. H. Otten, and H. J. L. J. Van der Linden, "Evaluation of Process Models for Fouling Control of Reverse Osmosis of Cheese Whey," *J. Membr. Sci., 58,* 89 (1991).
22. V. Gekas and B. Hallström, "Mass Transfer in the Membrane Concentration Polarization Layer under Turbulent Cross Flow. I. Critical Literature Review and Adaptation of Existing Sherwood Correlations to Membrane Operations," *30,* 153 (1987).
23. C. M. Tam and A. Y. Tremblay, "Membrane Pore Characterization—Comparison between Single and Multicomponent Solute Probe Techniques," *J. Membr. Sci., 57,* 271 (1991).

Received by editor March 2, 1992